

Towards anti-causal Green's function for three-dimensional sub-diffraction focusing

Guancong Ma^{1,2,4,5*}, Xiyang Fan^{2,5}, Fuyin Ma², Julien de Rosny³, Ping Sheng^{1,2*} and Mathias Fink^{1,3*}

In causal physics, the causal Green's function describes the radiation of a point source. Its counterpart, the anti-causal Green's function, depicts a spherically converging wave. However, in free space, any converging wave must be followed by a diverging one. Their interference gives rise to the diffraction limit that constrains the smallest possible dimension of a wave's focal spot in free space, which is half the wavelength. Here, we show with three-dimensional acoustic experiments that we can realize a stand-alone anti-causal Green's function in a large portion of space up to a subwavelength distance from the focus point by introducing a near-perfect absorber for spherical waves at the focus. We build this subwavelength absorber based on membrane-type acoustic metamaterial, and experimentally demonstrate focusing of spherical waves beyond the diffraction limit.

Causality in physics dictates that three-dimensional (3D) radiation of a point source is given only by the causal (or retarded) Green's function G_c (refs^{1,2}), which describes an outgoing wave. On the other hand, despite the fact that the anti-causal (or advanced) Green's function G_a is also a solution to the same wave equation, a converging wave alone is never observed. As a converging wave cannot stop in free space, it collapses at the focus and will continue its propagation as another diverging wave (Fig. 1a). Therefore, in 3D space, any converging monochromatic spherical wave $\phi_{cg} = G_a = \exp(-ikr - i\omega t)/r$ that focuses at the origin ($r=0$) is followed by a diverging wave (with a reverse sign) that reads $\phi_{dg} = G_c = \exp(ikr - i\omega t)/r$. Therefore, the total wave field is given by the superposition of these two waves

$$\phi = G_a - G_c = \left(\frac{e^{-ikr}}{r} - \frac{e^{ikr}}{r} \right) e^{-i\omega t} = -\frac{2i \sin(kr)}{r} e^{-i\omega t} \quad (1)$$

The minus sign in front of G_c accounts for the fact that, in free space, the two waves must destructively interfere, so that no singularity occurs. The amplitude of the total field has a sinc-function shape, as plotted in Fig. 1b as a function of r . We observe a main peak of full-width at half-maximum (FWHM) of $\sim \lambda/2$, surrounded by side-lobes that decay as r^{-1} . Such a shape is the consequence of the interference between G_a and G_c (refs^{2,3}). This is, in fact, the origin of the diffraction limit of a focal spot. How to focus beyond the diffraction limit is a topic of importance both fundamentally and for applications. An interpretation of sub-diffraction focusing is through the consideration of high spatial frequency. As plane-wave solutions of wave equations associated with high spatial frequency are evanescent and therefore cannot propagate, they cling to the near-field of a surface, and are missing in the far field of any lens. Many approaches have been proposed to overcome this limitation by reintroducing the evanescent waves to the near field of the desired focus, especially by metamaterials made of subwavelength resonators⁴. Examples include negative-index materials as superlenses^{5,6}, structures with hyperbolic dispersion as hyperlenses^{7,8} or resonant metalenses that possess polariton-like dispersion^{9,10}.

Here, we demonstrate a different kind of sub-diffraction focusing by building a stand-alone anti-causal Green's function G_a in 3D space up to a distance $a \ll \lambda$ from the origin. We achieve this by combining the power of a time-reversal (TR) mirror and a sub-wavelength near-perfect absorber for spherical waves of radius a . We show the way high absorption can play a positive role in a 3D focusing problem. This is particularly interesting, since absorption has been a common issue limiting the performance and practical use in previous examples of metamaterials.

Results

We begin by taking a closer look at equation (1), which suggests the possibility to manipulate the shape of the focal spot. Imagine the extreme case that $G_c = 0$, then the total field becomes $\phi = G_a$ (refs^{2,3}), as shown in Fig. 1c. Its amplitude becomes r^{-1} , which is divergent at the origin. Consequently, the FWHM of the focal spot is infinitely small. This is plotted in Fig. 1d. However, since the wave equation and therefore its solutions must be continuous everywhere, singularity in a wavefunction is forbidden in homogeneous media. Therefore, to have $G_c = 0$ implies one also has to time-reverse the source in addition to the waves. This implies the presence of a point sink at the origin, at which waves become extinct. Here, a sink is the time-reversed version of a source. By including the point sink, which takes the form of a delta function in real space in the source term of the wave equation, a wave singularity is then allowed. The evanescent components needed for the singularity are introduced by the time-reversed source (see Supplementary Notes and Supplementary Fig. 1 for more details). Sadly, in reality a point sink with infinitesimal dimension does not exist. Nevertheless, can we benefit from such an approach, and seek to reduce the size of a focal spot by creating a wave that mimics the anti-causal Green's function up to a finite distance $a \ll \lambda$ from the focus?

Building anti-causal Green's function in causal physics. To achieve this goal in a causal system, we identify two essential ingredients. The first one is the creation of a converging spherical wave. This is possible by using a TR mirror for acoustic waves^{11,12}. In particular, the existence of monopole radiation in 3D free space makes

¹Institute for Advanced Study, Hong Kong University of Science and Technology, Kowloon, Hong Kong, China. ²Department of Physics, Hong Kong University of Science and Technology, Kowloon, Hong Kong, China. ³Institut Langevin, CNRS, ESPCI Paris, PSL Research University, Paris, France.

⁴Present address: Department of Physics, Hong Kong Baptist University, Kowloon Tong, Hong Kong, China. ⁵These authors contributed equally: Guancong Ma, Xiyang Fan. *e-mail: phgma@hkbu.edu.hk; sheng@ust.hk; mathias.fink@espci.fr

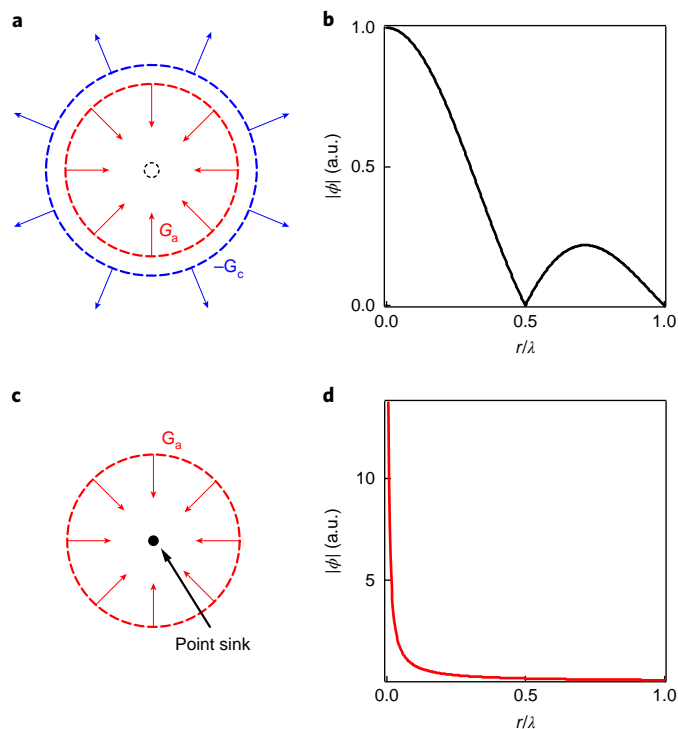


Fig. 1 | Formation of a focal spot. **a**, In free space, a spherical wave (red, described by the anti-causal Green's function G_a) converges to a point and subsequently becomes a diverging wave (blue, described by the causal Green's function G_c). **b**, Their interference gives rise to a total wave field that has a sinc-function shape, which is the hallmark of a focal spot. **c**, If a point sink is placed at the centre of the focal spot to remove the diverging wave but does not affect the converging wave, then the total wave field is given only by G_a . **d**, The focal spot has a singularity at the origin, and does not have any side-lobe.

acoustic waves the best candidate for this investigation, compared with electromagnetic waves, whose lowest possible radiation order in three dimensions is dipole¹³. The second ingredient is the design of a subwavelength object of radius a that behaves as a sink to annihilate the diverging wave, so that G_a can describe the total field in 3D space up to the radial position $r = a$. For monochromatic waves, such a subwavelength perfect absorber can be described as a spherical object with a surface impedance that is perfectly matched to a spherical converging wave at the radial position $r = a$. As the impedance for a spherical wave is a complex function of both frequency and radial position (see Supplementary Notes), both the real part and the imaginary part have to be matched.

This seemingly stringent requirement can now be met, owing to the recent advances in metamaterials. In particular, a new class of acoustic metamaterials^{14–21} with subwavelength dimensions demonstrate near-perfect absorption for acoustic plane waves. However, all of these solutions have been proposed and tested only for normal incidence of plane waves. Here, we choose a membrane absorber as a starting point. The physics and performance of the membrane absorber are detailed in ref.¹⁶. Simply put, this membrane absorber relies on the hybridization of at least two eigenmodes to attain impedance matching to incoming plane waves in air, and simultaneously possesses large evanescent components. Consequently, far-field reflection is minimized, and meanwhile the local energy density, and thereby the dissipative power, is maximized.

Subwavelength near-perfect absorber for a spherical wave. The main challenge is how to extend this concept to build a perfect

absorber in three dimensions to handle spherical waves that mimics a subwavelength sink. To begin, we need a structure whose symmetry is close to the spherical one. Here we choose to use a dodecahedron geometry consisting of 12 identical units of membrane absorber, each with the shape of a penta-pyramid. A photographic image is shown in the inset of Fig. 2a (see Methods for further details). The properties of this unit under plane-wave incidence are shown in Supplementary Fig. 2. The penta-pyramid absorbers can be easily assembled to a dodecahedron with a radius of $a = 4$ cm. The geometric shape of a dodecahedron suggests that it can potentially be a good absorber for a converging spherical wave. Yet characterization of its absorption for a spherical wave is an experimental challenge.

This brings us to the other ingredient central to our investigation, the generation of a converging spherical wave using a TR mirror²². We conduct the TR acoustic experiment in our laboratory, which is a reverberant room. In the first step, a short pulse is emitted by a monopole source (loudspeaker) placed in an empty part of the laboratory. The source position is defined as the origin ($r = 0$). The wave field is recorded by 16 microphones placed around the laboratory. (An alternative method exists for this step, see Methods for details.) In the second step of the experiment, the recorded signals are flipped in time in a computer and then emitted by 16 loudspeakers that are placed at the same positions as the microphones. The TR invariance guarantees that these waves will retrace their original propagation paths to converge to the origin, and reconstruct the pulse. Since the source is a monopole (which is removed in the back-propagation step), the TR wave field will focus isotropically, generating a spherical wave that converges to the origin.

We next seek to measure the absorption coefficient. To do so, we need to exploit the spatio-temporal characteristic of the TR re-focusing. As a short pulse was sent in the first step, the TR revival waves must collapse to the origin at a specific instant. Experimentally, this instant is given by the peak in the temporal signal recorded at the origin. (See Supplementary Fig. 3 for the signal we used.) This well-defined and easily identifiable focus time, which we denote $t = 0$, provides a clear separation of the incoming and outgoing waves at the origin. Waves converge to the origin for $t < 0$, and diverge for $t > 0$. By taking into account the acoustic time of flight, it is also easy to perform such a separation for TR signals measured in the vicinity of the origin.

To measure the absorption performance of the dodecahedral absorber, during the second step of the TR experiment, we arrange 12 miniature microphones on a semicircular arc to form a sensor array, whose centre coincides with the origin, as shown in Fig. 2a. The array can rotate to sweep a spherical surface that encloses the absorber, which is kept stationary. By recording the signals of TR re-focusing, and separating converging and diverging waves in the time domain, we are able to measure how much acoustic energy exits through the spherical surface formed by the microphone array. We measured the diverging waves for the cases with and without the absorber. The results are shown in Fig. 2b. Here the curves are the average of all 12 microphones. The radial axis represents the pressure amplitude, and the angular axis represents the array's angular position during the sweep. Without the absorber, the measured results (black curve) delineate a circle, which clearly indicates the isotropic nature of the spherical diverging waves. With the absorber, the outgoing energy is significantly reduced, as shown by the red curve. From this result, it is straightforward to obtain the experimental absorption coefficient α of the dodecahedral absorber, which, in this case, is $\alpha = 0.92$ at 795 Hz.

The absorption is high, but does not reach unity. This means that the dodecahedron is not perfectly matched to the converging wave impedance; and that there is a non-zero reflected wave, with the reflection coefficient between converging and diverging waves given by $R = e^{i\theta} \sqrt{1 - \alpha}$, where $|R| = \sqrt{1 - \alpha}$ is the amplitude and θ

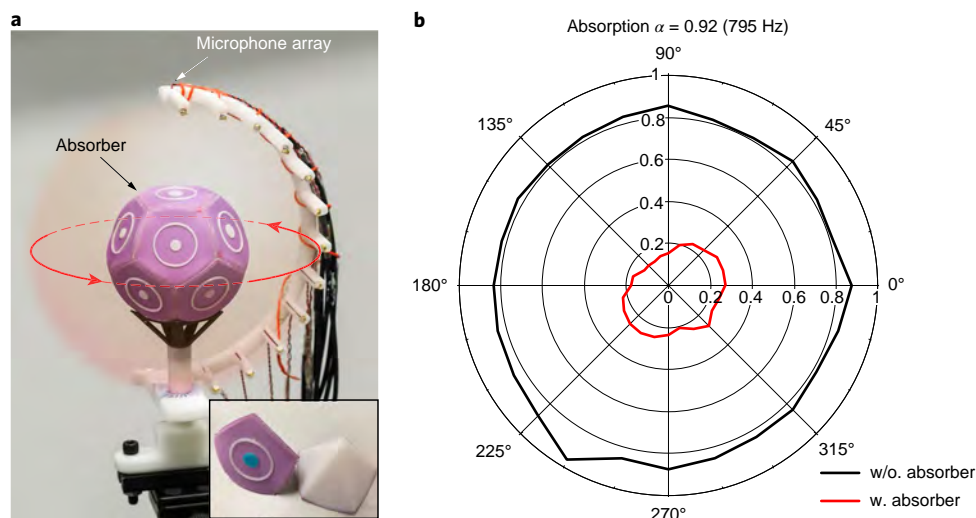


Fig. 2 | An absorber for converging spherical waves. **a**, The experimental set-up for the measurement of the absorption coefficient for spherical-wave incidence. The absorber for converging spherical waves, which is a dodecahedron of 12 identical unit membrane absorbers (inset), is placed at the centre of a half-circular microphone array. A spherical wave is converged to the centre of the absorber by a TR mirror. We rotate the microphone array to sweep a spherical surface (the reddish halo). We record the diverging wave that exits this enclosing surface. **b**, The measured results. The black curve is without the absorber, and the red curve is with the absorber. The radial axis represents the normalized pressure amplitude, and the angular axis is the array's azimuthal position. Here the results are the average of all the microphones on the array. It is seen that the absorber is able to remove a majority of the outgoing wave. Our measurement gives an absorption coefficient $\alpha = 0.92$ at 795 Hz.

is the reflection phase. Since most outgoing energy is removed, the total field, although not strictly G_a , becomes

$$\phi = G_a + RG_c = \frac{e^{-ikr}}{r} + e^{i\theta} \sqrt{1-\alpha} \frac{e^{ikr}}{r} \quad (2)$$

As we will show next, θ can be obtained from fitting the measured focal spot profile.

Sub-diffraction focusing. The high absorption must have a strong impact on the shape of the focal spot. To observe this, we scan the field along the radial direction, as shown in Fig. 3a. We point out that unlike for the measurement of the absorption coefficient, we now keep all temporal signals to obtain the total field, which include both $t < 0$ (converging) and $t > 0$ (diverging). The measured results are shown in Fig. 3b as markers. The black open markers delineate the case in which the absorber is absent. A well-defined standard focus is observed, which has the sinc-function shape. In the presence of the absorber (red markers), the focal spot has a very different shape. First, the main peak becomes more slender. The amplitude FWHM, calculated only from the maximal measured value measured outside the absorber (0.83, at $r/\lambda \sim 0.12$), is reduced to 0.4 λ , which is marked by the red arrow in Fig. 3b. This shows that the focal spot is now 20% smaller than the diffraction limit. Second, the first side-lobe is considerably suppressed, with a flatter profile and much smaller undulation.

The experimental result can be nicely fitted using equation (2) with the experimentally measured absorption $\alpha = 0.92$, and a fitting reflection phase $\theta = \pi$, as plotted in Fig. 3b by the red curve. Notably, with $\theta = \pi$, we can rewrite equation (2) as

$$\phi = \frac{e^{-ikr}}{r} - \sqrt{1-\alpha} \frac{e^{ikr}}{r} \quad (3)$$

by which we recover the form of equation (1). As a reference, the black curve in Fig. 3b is plotted from equation (3) with $\alpha = 0$.

The perfect spherical impedance matching will need $Z_s = -Z_{cg}$, where Z_s is the surface impedance of the absorber and Z_{cg} is the spherical converging wave impedance (details of the derivation are presented in Supplementary Notes). We can calculate that at $r = a = 4$ cm and $f = 795$ Hz, $-Z_{cg} = Z_0(0.25 + 0.43i)$, where $Z_0 = \rho_0 c_0$ is the characteristic impedance of air, with ρ_0 and c_0 being the mass density and speed of sound, respectively. Combining experimentally measured $|R| = \sqrt{1-\alpha} = 0.283$ and the fitting phase $\theta = \pi$, we can obtain $Z_s \approx Z_0(0.29 + 0.28i)$, which suggests that the absorber is well matched to $-Z_{cg}$ in the real part, but has a mismatch in the imaginary part. Nevertheless, our measurement already shows that due to the high absorption, the total field is dominated by G_a in $r > 4$ cm.

We have also carried out control experiments. It is seen that at frequencies with very small absorption, the dodecahedron has almost no effect on the shape of the focal spot. The results are shown in Supplementary Fig. 4.

From equation (3), one can easily see that even with a non-unity absorption coefficient, there is a component that yields a singularity at the origin. Unfortunately, this cannot be observed since equation (3) is satisfied only up to the absorber's surface at $a = 4$ cm. In addition, since the absorber still has a finite volume, singularity does not emerge in our system. We nevertheless use miniature microphones to measure inside the absorber, as shown in the inset of Fig. 3a. The measured results, together with the scanned wave field outside the absorber, are shown in Fig. 3c in a semi-log scale. It is seen that the wave amplitude inside the absorber is over one order of magnitude larger than that outside it. Yet this large wave magnitude is the consequence of the absorber's resonance. Indeed, we see in Fig. 3c that inside the absorber, the wave field distribution does not follow the theoretical curve (red) that is given by equation (3) by setting $\alpha = 0.92$. However, this information hints at an effective way to further reduce the size of the focal spot, which is to reduce the size of the absorber, which is achievable as long as the spherical impedance matching condition is satisfied.

The resonant nature of the absorber and the dispersive nature of the spherical impedance imply that the good impedance matching

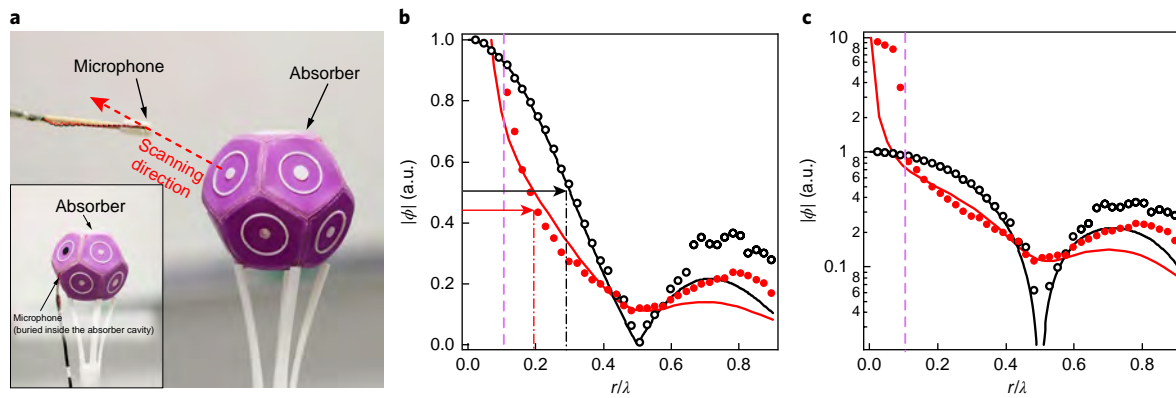


Fig. 3 | Focal spot in the presence of the absorber. **a**, A photograph of the experimental set-up to characterize the shape of the focal spot. A spherical wave converges to focus at the centre of the absorber. A microphone is mounted on a translation stage to measure the pressure field along the radial direction. **b,c**, The results at 795 Hz (that is, the frequency of the absorption peak). The black open circles show the focal spot in free space. The red filled circles are the focal spot in the presence of the absorber. Arrows and dotted-dashed lines mark half of the FWHM for each case. The purple dashed lines delineate the position of the surface of the absorber. **c**, In semi-log scale, the measured field both inside and outside the absorber using the set-up shown in the inset of **a**. The curves in **b** and **c** are theoretical predictions plotted by equation (3) with the experimentally measured absorption coefficient ($\alpha=0$ for the black curves, $\alpha=0.92$ and a fitting phase $\theta=\pi$ for the red curves). Good agreement is seen for the wave field outside the absorber.

as described above may not be achieved at frequencies other than 795 Hz. At other frequencies, the same absorber may give different α and θ . In particular, the phase factor θ can have interesting effects on the shape of the focal spot³. An investigation on this matter is detailed in Supplementary Fig. 5. and Supplementary Notes.

To further show that the resolution can indeed be improved via absorption, we use the TR technique to generate two identical, simultaneous and isotropic focal spots with a subwavelength separation of 0.4λ , as shown in Fig. 4a. We scan the field along the line connecting the two focus points. A single broad peak is the result, as shown in Fig. 4b as black open markers. Clearly, the focal spots cannot be resolved in free space. We then place two identical absorbers precisely at the two focal spots (Fig. 4a). In this case, the two focal spots are now easily distinguishable in the experiment (red markers, Fig. 4b), showing a substantial increase in resolution.

Discussion

The fundamental importance of a sink is also reflected in a recent debate on super-resolution in a positive-index medium^{23–25}. We

can reinterpret our experiment as a perfect TR experiment²⁶, and compare it to an ‘active sink’ that was experimentally demonstrated previously². The active sink was proposed to achieve a perfect TR experiment with elastic waves in two dimensions, which requires one to time-reverse not only the field (with a TR mirror)^{12,22,27–29}, but also the original source. An active sink achieves this by means of injecting another diverging wave during the TR step at the appropriate time, so that it exactly cancels the natural outgoing wave. Such an active sink has the advantage to work in an arbitrarily broad bandwidth. However, it requires a second injection of the original emission, which must contain all of the information about the pulse waveform, the knowledge of the instantaneous phase and the temporal information of the re-focusing. In comparison, what we show here in three dimensions is that for a narrow-band signal a passive sink can achieve a similar effect by absorbing almost all of the incoming energy of the converging wave. The result is a near-perfect time-reversed movie of the original experimental history, which consists of the emission by the source, followed by the wave’s propagation.

Our approach is also related to the use of coherent perfect absorbers³⁰, especially to the use of a time-reversed laser. Indeed, the relation between gain and loss is similar to the TR pair of source and sink. A coherent perfect absorber has been successfully demonstrated in experiments in a number of 1D systems^{31–34}, but its full potential in handling 3D wave fields remains beyond reach. Our absorber demonstrates near-unity absorption in three dimensions. Further improvement on the absorption performance may be possible by considering objects with exact spherical symmetry. For example, bubbles²¹ and porous silicone spheres³⁵ may be good candidates for ultrasound.

On another note, by realizing sub-diffraction focusing, our experiment indicates that subwavelength perfect absorbers can have a complex impact on the local shape of 3D wave fields. This phenomenon is very different from 1D systems, in which the main outcome of perfect absorption is the elimination of waves. Through careful design, strategically introduced subwavelength 3D perfect absorbers may generate a desirable wave field by the selective removal of waves from the system. To expand on this idea, we can even envision a new class of metamaterials that consist of either exclusively subwavelength absorber building blocks, or specific combinations of absorbers and scatterers, arranged in a lattice or in disorder. Their potential to manipulate and control wave propagation invites further investigations in the future.

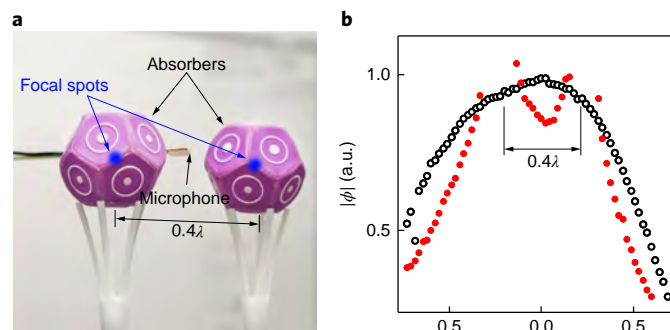


Fig. 4 | Improving resolution with absorbers. **a**, Two simultaneous focal spots with a subwavelength separation of 0.4λ are generated using the TR mirror. Two absorbers are placed at the positions of the two focal spots as shown. **b**, The measured results along the line that connects the centres of the two absorbers. The two focal spots are easily distinguishable when the absorbers are present (red circles). They cannot be resolved in the absence of the absorbers (black open circles).

We have presented a clear physical demonstration of the creation of an anti-causal Green's function in a large portion of 3D space. This leads to an interesting way to use a passive subwavelength absorber to focus wave energy to subwavelength scales, which can be useful for many applications where high energy density in a small region is desirable, such as lithography, seismology, ultrasonic cutting and ultrasonic scalpels. We may also ask the question of whether this concept can also be useful for better spatial resolution in imaging. The answer is not simple. In our approach, the exact positioning of the absorber at the point where the converging wave focuses is a key point. However, the imaging process is very different. To make an image from the object's scattered field, we have to back-propagate this field to build the image. This step is usually performed in a computer by software (digital holography). Therefore, as the exact shape and position of the object is unknown, it is very difficult to compute a perfect absorber exactly matched to the object shape³⁶. However, for sparse objects made of a limited number of point scatterers, this concept can be of interest to better localize each scatterer.

Methods

Methods, including statements of data availability and any associated accession codes and references, are available at <https://doi.org/10.1038/s41567-018-0082-3>.

Received: 4 August 2017; Accepted: 13 February 2018;

Published online: 19 March 2018

References

- Feynman, R. P., Leighton, R. B. & Sands, M. *The Feynman Lectures on Physics* Vol. II (Basic Books, New York, NY, 2011).
- de Rosny, J. & Fink, M. Overcoming the diffraction limit in wave physics using a time-reversal mirror and a novel acoustic sink. *Phys. Rev. Lett.* **89**, 124301 (2002).
- Noh, H., Popoff, S. M. & Cao, H. Broadband subwavelength focusing of light using a passive sink. *Opt. Express* **21**, 17435–17446 (2013).
- Maznev, A. A. & Wright, O. B. Upholding the diffraction limit in the focusing of light and sound. *Wave Motion* **68**, 182–189 (2017).
- Pendry, J. B. Negative refraction makes a perfect lens. *Phys. Rev. Lett.* **85**, 3966 (2000).
- Kaina, N., Lemoult, F., Fink, M. & Lerosey, G. Negative refractive index and acoustic superlens from multiple scattering in single negative metamaterials. *Nature* **525**, 77–81 (2015).
- Li, J., Fok, L., Yin, X., Bartal, G. & Zhang, X. Experimental demonstration of an acoustic magnifying hyperlens. *Nat. Mater.* **8**, 931–934 (2009).
- Shen, C. et al. Broadband acoustic hyperbolic metamaterial. *Phys. Rev. Lett.* **115**, 254301 (2015).
- Lemoult, F., Lerosey, G., de Rosny, J. & Fink, M. Resonant metalenses for breaking the diffraction barrier. *Phys. Rev. Lett.* **104**, 203901 (2010).
- Zhu, J. et al. A holey-structured metamaterial for acoustic deep-subwavelength imaging. *Nat. Phys.* **7**, 52–55 (2011).
- Fink, M. Time reversed acoustics. *Phys. Today* **50**, 34–40 (2008).
- Yon, S., Tanter, M. & Fink, M. Sound focusing in rooms: The time-reversal approach. *J. Acoust. Soc. Am.* **113**, 1533–1543 (2003).
- Jackson, J. D. *Classical Electrodynamics* (Wiley, New York, NY, 2007).
- Cummer, S. A., Christensen, J., Springer, A. & Alù, A. Controlling sound with acoustic metamaterials. *Nat. Rev. Mater.* **1**, 16001 (2016).
- Ma, G. & Sheng, P. Acoustic metamaterials: From local resonances to broad horizons. *Sci. Adv.* **2**, e1501595 (2016).
- Ma, G., Yang, M., Xiao, S., Yang, Z. & Sheng, P. Acoustic metasurface with hybrid resonances. *Nat. Mater.* **13**, 873–878 (2014).
- Mei, J. et al. Dark acoustic metamaterials as super absorber for low-frequency sound. *Nat. Commun.* **3**, 756 (2012).
- Li, Y. & Assouar, B. M. Acoustic metasurface-based perfect absorber with deep subwavelength thickness. *Appl. Phys. Lett.* **108**, 063502 (2016).
- Yang, M., Chen, S., Fu, C. & Sheng, P. Optimal sound-absorbing structures. *Mater. Horiz.* **4**, 673–680 (2017).
- Cai, X., Guo, Q., Hu, G. & Yang, J. Ultrathin low-frequency sound absorbing panels based on coplanar spiral tubes or coplanar Helmholtz resonators. *Appl. Phys. Lett.* **105**, 121901 (2014).
- Leroy, V. et al. Superabsorption of acoustic waves with bubble metascreens. *Phys. Rev. B* **91**, 020301 (2015).
- Fink, M. et al. Time-reversed acoustics. *Rep. Prog. Phys.* **63**, 1933–1995 (2000).
- Leonhardt, U. Perfect imaging without negative refraction. *New J. Phys.* **11**, 093040 (2009).
- Ma, Y. G., Sahebdivan, S., Ong, C., Tyc, T. & Leonhardt, U. Evidence for subwavelength imaging with positive refraction. *New J. Phys.* **13**, 033016 (2011).
- Tyc, T. & Zhang, X. Perfect lenses in focus. *Nature* **480**, 42–43 (2011).
- Fink, M., de Rosny, J., Lerosey, G. & Tourin, A. Time-reversed waves and super-resolution. *C. R. Phys.* **10**, 447–463 (2009).
- Draeger, C. & Fink, M. One-channel time reversal of elastic waves in a chaotic 2D-silicon cavity. *Phys. Rev. Lett.* **79**, 407–410 (1997).
- Lerosey, G. et al. Time reversal of electromagnetic waves. *Phys. Rev. Lett.* **92**, 193904 (2004).
- Przadka, A. et al. Time reversal of water waves. *Phys. Rev. Lett.* **109**, 064501 (2012).
- Chong, Y. D., Ge, L., Cao, H. & Stone, A. D. Coherent perfect absorbers: time-reversed lasers. *Phys. Rev. Lett.* **105**, 053901 (2010).
- Wan, W. et al. Time-reversed lasing and interferometric control of absorption. *Science* **331**, 889–892 (2011).
- Li, S. et al. Broadband perfect absorption of ultrathin conductive films with coherent illumination: Superabsorption of microwave radiation. *Phys. Rev. B* **91**, 220301 (2015).
- Meng, C., Zhang, X., Tang, S. T., Yang, M. & Yang, Z. Acoustic coherent perfect absorbers as sensitive null detectors. *Sci. Rep.* **7**, 43574 (2017).
- Pirruccio, G., Martín Moreno, L., Lozano, G. & Gómez Rivas, J. Coherent and broadband enhanced optical absorption in graphene. *ACS Nano* **7**, 4810–4817 (2013).
- Brunet, T. et al. Soft 3D acoustic metamaterial with negative index. *Nat. Mater.* **14**, 384–388 (2014).
- Assous, F., Kray, M., Nataf, F. & Turkel, E. Time-reversed absorbing condition: application to inverse problems. *Inverse Probl.* **27**, 065003 (2011).

Acknowledgements

G.M. and P.S. acknowledge the support of the Hong Kong Research Grants Council (grant no. AoE/P-02/12). J.d.R. and M.F. acknowledge LABEX WIFI (Laboratory of Excellence within the French Program Investments for the Future) under references ANR-10-LABX-24 and ANR-10-IDEX-0001-02 PSL*.

Author contributions

M.F., G.M. and P.S. supervised the research. G.M. designed the experiment with the help of J.d.R. X.F. and G.M. carried out the experiment. F.M. performed experiments at the early stage of this project. All authors were involved in discussion and analysis of data. G.M., P.S. and M.F. prepared the manuscript.

Competing interests

The authors declare no competing interests.

Additional information

Supplementary information is available for this paper at <https://doi.org/10.1038/s41567-018-0082-3>.

Reprints and permissions information is available at www.nature.com/reprints.

Correspondence and requests for materials should be addressed to G.M. or P.S. or M.F.

Publisher's note: Springer Nature remains neutral with regard to jurisdictional claims in published maps and institutional affiliations.

Methods

Time-reversal experiment. We perform the TR experiment for airborne sound in our laboratory room¹², which has dimensions of 9.0 m (length) \times 6.0 m (width) \times 4.5 m (height). At 800 Hz, the room is in the reverberant regime³⁷. A reverberant room is ideal for TR re-focusing experiments, compared with an anechoic chamber. In an anechoic chamber, a large spatial sampling rate, and therefore an unrealistically large number of sensor/speaker channels, are required to completely cover the enclosing surface of the source. In a reverberant room, the sound emitted by the source is multiply scattered by the boundaries and various objects. Consequently, waves take multiple paths to arrive at any microphone. As a result, a very long signal (coda) is recorded with each microphone, which contains information about waves arriving via multiple different paths. A direct consequence is that the spatial sampling rate can be drastically reduced. Therefore, we are able to perform a near-perfect TR experiment with only 16 channels of speakers/sensors³⁷.

The TR experiment consists of two steps. There are two alternative methods for the first step. In the first method, a short pulse is emitted by a monopole source, which is an omni-directional speaker assembly placed in an empty part of the laboratory. The speaker has the same size as the absorber. The emitted signal covers a bandwidth of 100–1,500 Hz. Sixteen microphones are placed around the laboratory to record the acoustic signals. The received signals, which are essentially the impulse responses of the room, consist of the sound that takes a direct path (from the speaker to one microphone), as well as the sound that has been multiply scattered off the walls and obstacles. In the second step of the experiment, we remove the omni-directional speaker. The recorded signals are flipped in time in a computer, and then emitted by another set of 16 loudspeakers that are placed at the same positions as the microphones. The TR invariance guarantees that these waves must retrace their original propagation paths to converge to the origin to reconstruct the pulse. As the original emission is a monopole radiation, the TR revival waves must focus isotropically in all spatial dimensions, forming a converging spherical wave.

The alternative method for the first step of the TR experiment is to exploit the spatial reciprocity of the wave equation. It tells us that the role of a source and a receiver can be reversed, giving rise to the same impulse response in any stationary medium. Therefore, for the measurement of the impulse response, the

position of the receiver and transmitter can be exchanged. To elaborate, emitting a short pulse from the source point x_s and recording with a microphone at X_m , we obtain the impulse response $G(x_s, X_m, t)$. (This is the way to measure the signals to be time-reversed in the method described above.) We can also directly use the loudspeaker located at position X_m as the source, and record the signal with one microphone located at x_s . The recorded signal is $G(X_m, x_s, t)$. Spatial reciprocity tells us $G(x_s, X_m, t) = G(X_m, x_s, t)$. Each loudspeaker emits individually, so that the microphone records 16 sets of signals, which are time-reversed for re-emission in the second step. The two techniques are equivalent, since the microphone we use is a monopolar one. This method also simplifies the experimental set-up by requiring only one microphone that is placed at the focus point. We have compared these two methods in experiments, and found almost no difference.

Membrane absorber. The membrane absorber consists of a decorated membrane, and a small air cavity behind it. Each membrane has the shape of a regular pentagon with a side length of 25 mm. It is evenly stressed and fixed at the edges; and is decorated by a circular platelet with a radius of 3.5 mm, weighing 0.05 g; and a plastic ring with an inner radius of 11 mm and an outer radius of 12 mm, weighing 0.15 g. The cavity, fabricated using 3D printing, is a pyramid with a height of 31 mm. The air cavity induces the membrane's second and third eigenmodes to hybridize, forming a new set of 'hybridized resonances', of which the membrane's vibration profiles are the superposition of the membrane's eigenmodes (Supplementary Fig. 2). Twelve identical units are assembled into a dodecahedron with a radius of 4 cm that has a symmetry close to a sphere. Our measurements show that the structure attains near-perfect absorption of spherical incident waves near 795 Hz.

Data availability. The data that support the plots within this paper and other findings of this study are available from the corresponding authors upon reasonable request.

References

37. Kuttruff, H. *Room Acoustics* (Taylor & Francis, New York, NY, 2009).